Article:

Rogers, M, Prokscha, T, Teobaldi, G et al. (2021) Observation of a molecular muonium polaron and its application to probing magnetic and electronic states. Physical Review B, 104 (6). 064429. ISSN: 2469-9950

https://doi.org/10.1103/PhysRevB.104.064429

Observation of a molecular muonium polaron and its application to probing magnetic and electronic states

M. Rogers[1*], T. Prokscha[2], G. Teobaldi[3,4,5], Leandro Liborio[3], S. Sturniolo[3], E. Poli[3], D. Jochym[3], R. Stewart[6†], M. Flokstra[6], S. Lee[6], M. Ali[1], B.J. Hickey[1], T. Moorsom[1§] and O. Cespedes[1*]

Muonium is a combination of first- and second-generation matter formed by the electrostatic interaction between an electron and an antimuon (μ^+). Although a well-known physical system, their ability to form collective excitations in molecules had not been observed. Here, we give evidence for the detection of a muonium state that propagates in a molecular semiconductor lattice via thermally activated dynamics: a muonium polaron. By measuring the temperature dependence of the depolarisation of the muonium state in C_{60}, we observe a thermal narrowing of the hyperfine distribution that we attribute to the dynamics of the muonium between molecular sites. As a result of the timescale for muonium decay, the energies involved, charge and spin selectivity, this quasiparticle is a widely applicable experimental tool. It is an excellent probe of emerging electronic, dynamic and magnetic states at interfaces and in low dimensional systems, where direct spatial probing is an experimental challenge owing to the buried interface, nanoscale elements providing the functionality localization and small magnitude of the effects.

I. Introduction

[1] *School of Physics and Astronomy, University of Leeds, Leeds LS2 9JT, United Kingdom.*[2]*Laboratory for Muon Spin Spectroscopy, Paul Scherrer Institute, 5232 Villigen, Switzerland.*[3] *Scientific Computing Department, Science & Technology Facilities Council, Rutherford Appleton Laboratory, Didcot OX11 0QX. United Kingdom.* [4] *Stephenson Institute for Renewable Energy, Department of Chemistry, University of Liverpool, Liverpool L69 3BX, United Kingdom.* [5]*School of Chemistry, University of Southampton, Highfield, Southampton SO17 1BJ, United Kingdom.* [6]*School of Physics and Astronomy, SUPA, University of St Andrews, St Andrews KY16 9SS, United Kingdom.*[†]*Current address: Laboratory for Mesoscopic Systems, Department of Materials, ETH Zurich, 8093 Zurich, Switzerland and Laboratory for Multiscale Materials Experiments, Paul Scherrer Institute, 5232 Villigen PSI, Switzerland.*[§]*Current address: Kelvin Building; University of Glasgow, Glasgow, G12 8QQ, United Kingdom.* **e-mail:M.D.Rogers@leeds.ac.uk; O.Cespedes@leeds.ac.uk*

The ability to map in a multi-layered thin film electronic, vibrational and spin order in thin films is key to many chemical, engineering and physical applications –in particular for compounds involving nanocarbon and molecular materials.[1,2] Yet, the direct spatial probing of spin ordering and electronic properties is an experimental challenge, owing to the nm-scale localisation and small magnitude of the effects. Magnetic proximity, spin accumulation and spontaneous spin order in non-magnetic metals can lead to localised magnetic phenomena that are at the lower limit of sensitivity of lab-based and synchrotron magnetometry techniques.[3-6] Mapping charge distribution is also an essential challenge to e.g. solid-state (thin-film) batteries and fullerene hybrid photovoltaics.[7,8] In the past, bulk muon spin rotation (μSR) has been used extensively to study various properties of the fullerenes including, but not limited to: rotational dynamics,[9,10] superconducting properties of the alkali-doped fullerene complexes[11] and spin ordering in the TDAE-C_{60} charge-transfer complex.[12]

Low-energy muon spin rotation (LE-μSR) is also a powerful tool in characterising interfacial and thin film spin phenomena for a multitude of systems.[13-16] Here, LE-μSR is used first to show the presence of low frequency endohedral muonium in C_{60}, coupled to the vibrational states of the molecule at all temperatures. The depolarisation of this state is linked to the dynamics of the molecular cages, as two distinct dynamical phases can be seen in the temperature dependence of this state. This muonium polaron is a highly sensitive probe to local electronic, vibrational and spin states. Here, we use it to probe changes in electron density at metal interfaces and emergent magnetism down to ~10s of μT via Zeeman splitting of the hyperfine interaction. The principle for this probing technique is shown in Fig. 1a.

II. Observation of the floating endohedral muonium polaron in C_{60} ($ENDO_f$)

The zero-field (ZF) muonium oscillation data for an amorphous, thick (∼200 nm) C_{60} film has been fitted using a multiple frequency model, where an individual precession frequency v_i has a contribution to the muon polarisation, $P(t)$, given by

$$P(t) = \sum_{i=1}^{4} A_i \cos(2\pi v_i t)\, e^{(-\lambda_i t)} \qquad (1)$$

λ_i is the depolarisation rate of the oscillating muonium. The asymmetry, A_i, is then the fraction of signal attributed to a given oscillation –see Supplemental Material [17].

At room temperature, C_{60} crystals form a face-centred cubic (fcc) structure where the individual molecules are orientationally disordered and freely rotate between degenerate configurations via a ratcheting mechanism.[18] Below 260 K, C_{60} molecules lose two rotational degrees of freedom. Due to inequivalent molecular orientations on the Bravais sites of the fcc lattice, crystalline C_{60} undergoes a first-order phase transition to a simple cubic structure. Below ~120 K, the time scale of the molecular rotation (τ_r) is longer than the measurement timescale for μSR ($\tau_m \sim$ 2.2 μs), and the rotational degrees of freedom appear frozen.[19,20] As shown in Fig. 1b, at low temperatures, oscillations at 1.2 MHz, 7.4 MHz and 8.6 MHz are visible. These frequencies are well understood and are attributed to the completely anisotropic hyperfine interaction of the exohedral radical muonium state (EXO),[21,22] but can only be detected when $\tau_r > \tau_m$.

In addition to the MuC_{60} radical precession, we observe an additional low-frequency precession that persists up to room temperature. This room-temperature oscillation has not been reported in the various studies of bulk crystalline C_{60}.[22,23] However, it is seen in all the thin fullerene films grown throughout this study, with stronger signals in the more disordered films. This high temperature muonium state has been shown to be sensitive to magnetic surface states.[3,4] The presence of the sub-MHz oscillation infers some intrinsic distortion of the fullerene cages and a precession decoupled from the molecular dynamics. Density Functional Theory (DFT) simulations of muon and muonium species in different crystalline C_{60} films,[17] identifies the $ENDO_f$ state as the energetically most favoured product of electron trapping at μ^+ sites in the presence of free-carriers in the conduction band of the C_{60} film ([17] Fig. S13 and Table S5), as produced by the μ^+ keV implantation. This polaronic state, with a formation energy of about -0.72 eV, is characterized by a floating geometry for the μ^+ inside the C_{60} ($ENDO_f$), slightly offset from the centre of mass of the C_{60} and at a distance of ~3 Å from the closest C-atom ([17] Fig. S7). As shown by the absence of μ^+-C stretching vibrational modes (Table S3), this geometry presents no chemical bonding between muonium and C_{60}, leading to an electron spin-density localised around the μ^+ sites ([17] Fig. S11).

The low-frequency oscillation is due to an axially symmetric hyperfine interaction for $ENDO_f$. Its frequency depends on film quality, charge state and the local magnetic field. It varies between 0.1 MHz for a highly crystalline, pristine and degaussed system, to 0.8 MHz for an amorphous, non-degaussed and/or charged film e.g. at metallic interfaces. This is in good agreement with the predicted value of ~0.45 MHz for a system with 25% C_{60}-vacancies (see Table S7 [17]). Experimentally, the formation energy of the $ENDO_f$ polaron is 300±100 meV (Figs. 1c-d). This is a factor two smaller than in the calculations (Table S5 [17]). The difference is probably due to impurities and defects up to 0.9 eV above the top of the valance band,[24] limitations in the simulations and the overestimated concentration of μ^+ in simulations with respect to the experiment, where only one μ^+ is present in the ~10^{-4} cm^3 sample at a time. The overestimated concentration induces unscreened, artificial electrostatic (multipolar) interactions between periodic replicas of the simulation cell that in turn over-stabilise the polaronic solution with respect to the delocalised state (Fig. 1c).

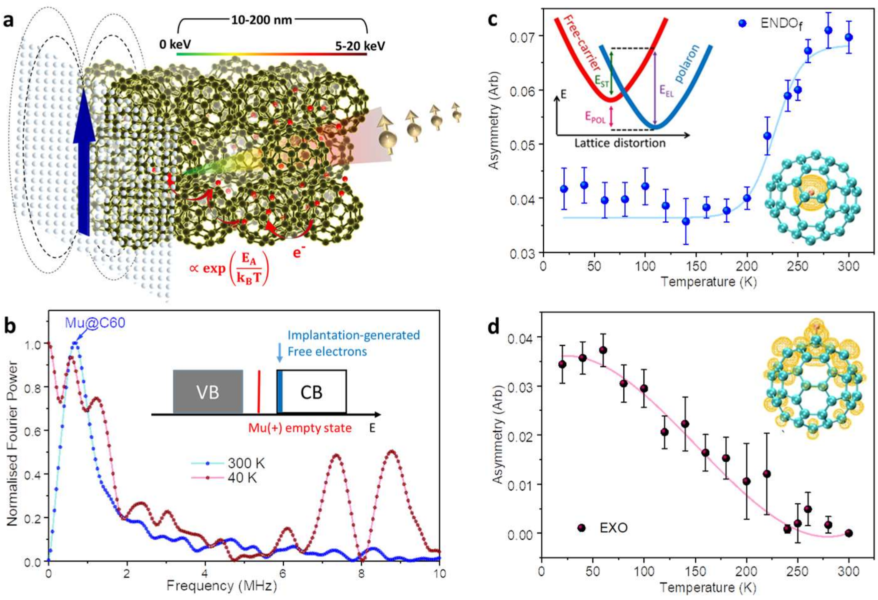

Figure 1. a. *Schematic of the ENDO$_f$ formation via ionisation, charge hopping and trapping then coupled with molecular rotations. Its oscillation frequency is sensitive to e.g. the electron transfer and emergent magnetism at interfaces.* ***b.*** *Fourier transform of the time domain asymmetry data at ZF for a 210 nm thick amorphous* C_{60} *film on a thermally oxidised Si substrate. The EXO muonium at 1.2, 7.4, and 8.6 MHz is observable at 40 K. At 300 K, only the ENDO$_f$ muonium is observed. Inset: (~keV) muon-beam generated free carriers remain delocalized in the conduction band (CB) of the* C_{60} *film, leaving the e-acceptor state of the* μ^+ *empty.* ***c.*** *The temperature dependence of the asymmetry attributed to the low-frequency ENDO$_f$ together with the calculated spin-density using the PBE exchange-correlation (XC) functional (yellow: 10^{-6} μ_B Å^{-3}). A semi-empirical model has been used to fit the temperature dependence leading to an activation energy (equivalent to –E_{POL}) for ENDO$_f$ of E_A =300±100 meV.[25]* ***d.*** *Temperature dependence of the EXO signal fraction, also with the calculated PBE spin-density (yellow: 10^{-6} μ_B Å^{-3}). The EXO state becomes more apparent as we cool the system through the glass transition and the molecular rotations are frozen.*

III. Dynamics of the ENDO$_f$ muonium polaron

Molecules in C_{60} films undergo a glass transition at $T_g \sim 120$ K. Below this temperature, the rotational degrees of freedom for the fullerene cages are completely frozen. Above T_g, a uniaxial ratcheting mechanism between different molecular orientations takes place until around 260 K, where the cages undergo continuous rotational diffusion.[26] Additionally, Born-Oppenheimer, DFT Molecular Dynamics (BOMD) simulations of different endohedral and exohedral μ^+ and muonium species confirm the ENDO$_f$ state as the only system uncorrelated to the C_{60} rotational dynamics. This makes ENDO$_f$ the only detectable oscillation at 250 K, regardless of the C_{60} free rotation. Path Integral MD (PIMD) simulations of the ENDO$_f$ state at 50 K and 300 K confirm its localisation around, but not exactly at, the centre of mass of the C_{60}. There is no quantum tunnelling through the C_{60} cage observed during the (finite) timespan of the simulations (Fig. 2c).

The depolarisation rate λ of the low-frequency oscillation was studied as a function of temperature T. We assume Arrhenius dynamics, with a decoherence period τ such that:[27]

$$\lambda \sim \frac{1}{\tau} = A e^{\frac{E_A}{k_B T}} \qquad (2)$$

Where E_A is the activation energy, k_B Boltzmanns constant and A a fitting factor. Although the ENDO$_f$ state appears decoupled from the molecular rotations in the ps scale (see Figs. 2a-c), we expect some effect of the ratcheting on the muonium spin direction over the longer decay timescale of 2.2 μs. The dynamics may have an effect in the temperature-dependent slowing of the decoherence.

The spin depolarisation of the ENDO$_f$ polaron state undergoes thermal changes with characteristic activation energies of the order of 15 meV above T_g and 1 meV below T_g (Fig. 2d). This observation resembles the temperature dependent, motional line-narrowing experienced in NMR experiments, where the increased motion of a sampling environment due to molecular dynamics causes areas of varying magnetic field to become more homogeneous, reducing the depolarisation of the nuclear spin.[28,29] The depolarization above T_g is therefore conditioned by the molecular rotations. Below T_g, the activation energy corresponds to the dynamic barrier for the movement and rotation of the muonium inside the cage, as observed in both the BOMD (Sup. Mat. Figs. S14-S15 [17]) and PIMD (Fig. 2c) simulations.

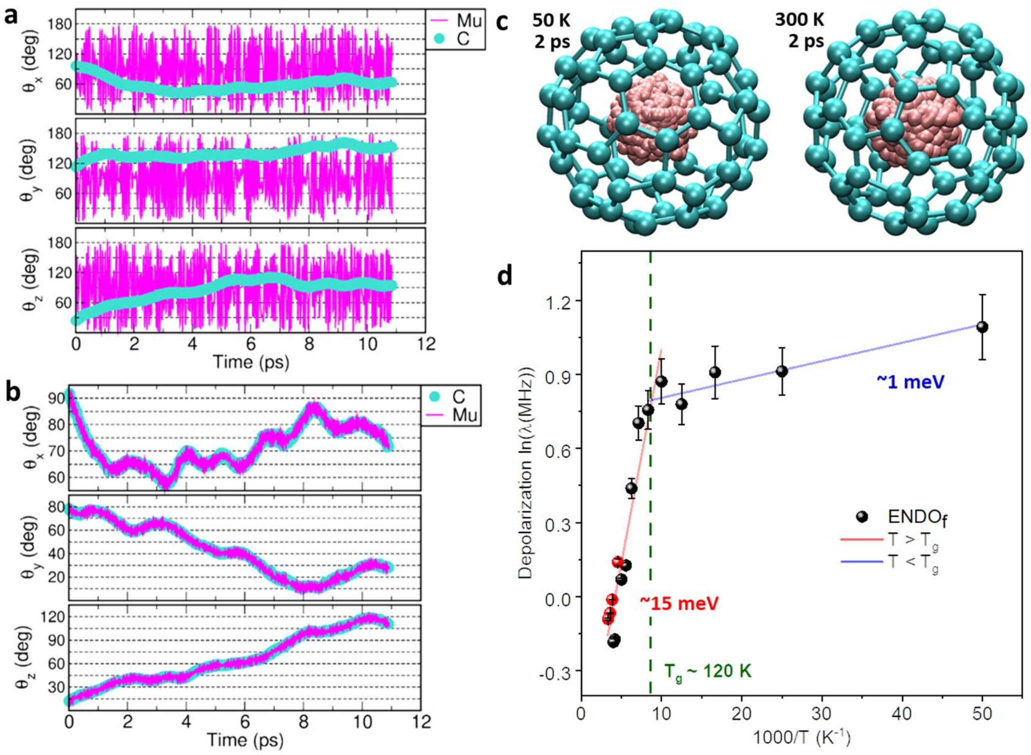

Figure 2. *Muonium dynamics and activation energies.* ***a.*** *Time evolution of the Mu- and C- rotational dynamics in ENDO$_f$, as calculated by the angles between the instantaneous Mu (closest C-atom) radial distance from the C_{60}'s centre of mass and the x (θ_x),y (θ_y) and z (θ_z) axes. The C-trace reports the rotational evolution of the C-atom closest (~3 Å) to the Mu at the start of the BOMD trajectory.* ***b.*** *As in a, but for the EXO muonium state. The C-atom closest to the Mu does not change during the whole BOMD trajectory. Note that for the ENDO$_f$ state the dynamics of molecule and muonium are decoupled, whereas in the EXO state the muonium follows the molecular rotation.* ***c.*** *Ab-Initio Path Integral Molecular Dynamics (AI-PIMD) distribution of the muon particle in the ENDO$_f$ at 50 K and 300 K. For each of the 16 beads used in the simulations, 1000 frames (2 fs apart) were extracted from the production run and superimposed in the same image. The initial position of the C_{60} is used to provide a better visualization of the quantum spread of the muonium inside the molecule. C: cyan, Mu: pink.* ***d.*** *Temperature dependence of the depolarisation rate associated with ENDO$_f$ state, showing the two thermal activation regimes above (red line fit) and below (blue) the glass transition T_g.*

IV. Low magnetic field detection in a crystalline sample

The dependence on the muonium hyperfine transition frequency upon magnetic field was studied using a crystalline C_{60} film grown at a substrate temperature of 473 K onto a [110] oriented Nb layer sputtered at 1073 K onto c-plane Al_2O_3 –XRD spectrum in Fig.S1. When comparing the crystalline C_{60} to the disordered film grown on SiO_2 at room temperature, we note that muonium formation is 30% of the implanted muons, demonstrating the diamagnetic behaviour of the uncoupled μ^+ particle. The difference suggests a role of the molecular crystal structure to the formation of the muonium polaron, as observed in the calculated vibrational DOS of C_{60} for crystalline and disordered films. This probably explains the discrepancy between these measurements and past studies on fullerite single crystals. Fig. 3 and Fig. S3 [17] demonstrate that at 250 K, in fields up to 8 G, there is only a single frequency line, increasing linearly at 1.402±0.003 $MHzG^{-1}$ [30]. This is in line with the standard theoretical predictions for a strongly coupled muon-electron system. Simultaneously, there is axial anisotropy leading to a zero-field frequency of 0.50±0.02 MHz. At 20 K, ν_{ZF} reduces to 0.15±0.03 MHz with the slope reducing to 0.74±0.05 $MHzG^{-1}$ (Fig. 3b). This slope cannot be explained by a simple 'strong coupling' approximation, which predicts the behaviour seen in Fig 3(a). It appears instead in the case of isotropic coupling on the same order of magnitude as the applied field, which suggests a small Fermi contact term for this site –see the Sup. Mat. for further detail.[17]

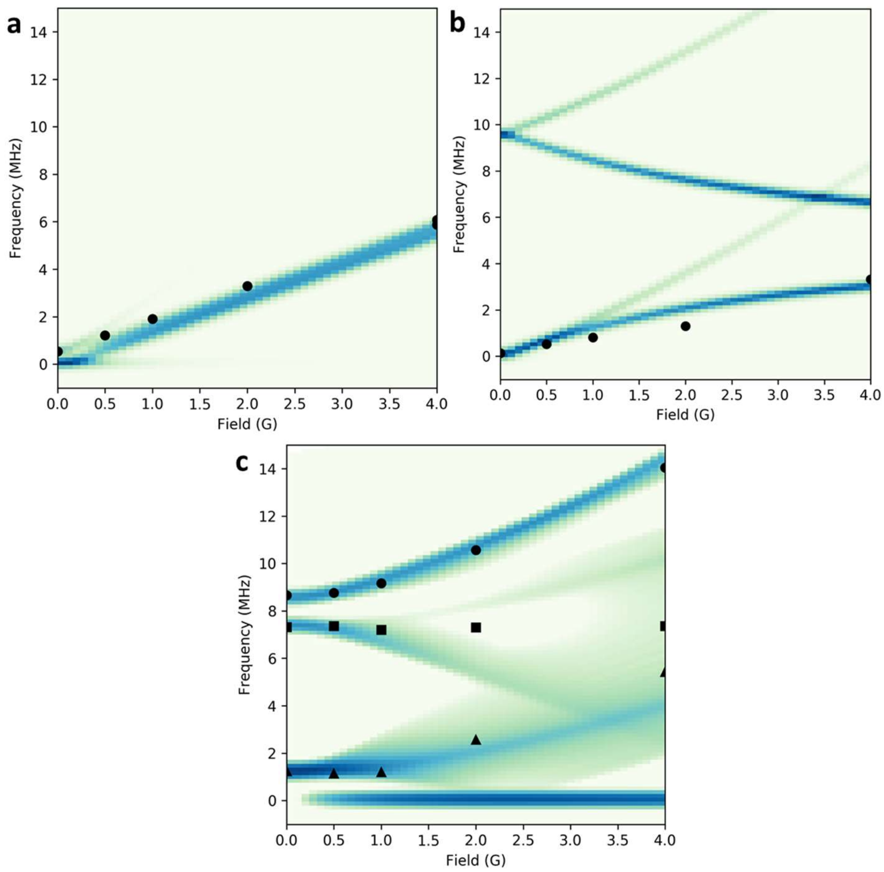

__FIG. 3.__ The magnetic field dependence of the ENDO$_f$ and EXO muonium oscillation frequencies as measured in the crystalline sample. __a.__ Observed experimental frequencies (circles) vs. simulations (colour map) for ENDO$_f$ at 250 K. __b.__ 20 K experiments (circles) and simulations (colour map) for the ENDO$_f$ state, modelled with a hyperfine isotropic coupling A_{iso} = 9.65 MHz. __c.__ Observed experimental frequencies (circles, squares and triangles) vs. simulated intensities (colour map) for the EXO state. The dipolar part of the tensor was chosen to match the observations at zero field and the Fermi contact term is in the high limit (A_{iso} >> 100 MHz). Since the middle peaks become very broad and low at high field, the colour map here is logarithmic in order to enhance their visibility. This decay with field is observed experimentally.[17]

V. Probing emergent local moments and electronic states at metallo-molecular heterostructures

We use the ENDO$_f$ state to detect small spin-electronic changes at a metallo-molecular interface. The sample structure is [Si(Sub)/Ta(3)/Cu(5)/C_{60}(114)/Cu(5)/Au(14)], where the thicknesses in brackets are in nm. Here, the Ta layer seeds the [111] growth of the Cu film. The thickness of the Au layer was chosen to provide adequate moderation of the muon beam, whilst also protecting the sample against oxidation. Measurements were taken at 250 K, where the time scale of the rotation of the molecule is short enough that the EXO muonium does not contribute to the observed signal. The sample was grown in a forming field of 20 mT. The sample was first measured in zero-field before any other magnetic field was applied. The time-dependent polarisation of the muonium state in ZF has been fitted with a single frequency model with the addition of an A_{tail} decay term which accounts for the slow depolarisation of diamagnetic μ+ particles within the metal layers:

$$P(t) = A_{Mu}\cos(2\pi v_{Mu}t)\, e^{(-\lambda_{Mu}\cdot t)} + A_{tail}e^{(-\lambda_{tail}\cdot t)} \qquad (3)$$

This yields the ENDO$_f$ oscillation frequency, υ_{Mu}. The depolarisation rate, λ_{Mu}, is also obtained. λ_{Mu} characterises the distribution of hyperfine oscillations contributing towards the signal at any given implantation energy. Fig. 4(b) shows the dependence of the percentage change in ENDO$_f$ frequency, $\Delta\upsilon_{Mu}$, as a function of implantation depth. The average implantation depth has been calculated from the simulated stopping profiles shown in Fig. 4(a). $\Delta\upsilon_{Mu}$ has been calculated relative to the frequency at 12 keV - the implantation energy that captures the centre-most region. In the initial, as-grown measurement, a curved profile of muonium frequency is observed with depth. υ_{Mu} is higher at the top and bottom interfaces by 14±5% and 25±5% respectively. From this measurement alone, it is clear that towards the C_{60}/Cu interfaces, there is a change in the hyperfine splitting between ENDO$_f$ spin configurations. Orbital re-hybridisation, lattice reconstruction and Fermi level matching, lead to charge-transfer from the metal into the first fullerene monolayer.[31-34] As the neutral C_{60} LUMO is triply degenerate, the addition of charge is accompanied by a molecular distortion to break the degeneracy through the Jahn-Teller effect.[35] The reduced symmetry due to the molecular distortion imparts anisotropy onto the hyperfine coupling tensor, which describes the energy splitting in zero-field of the triplet muonium spin configurations. This is the cause of the observable 0.7 MHz ZF oscillation in the oblate molecule, C_{70}.[9,10,36]

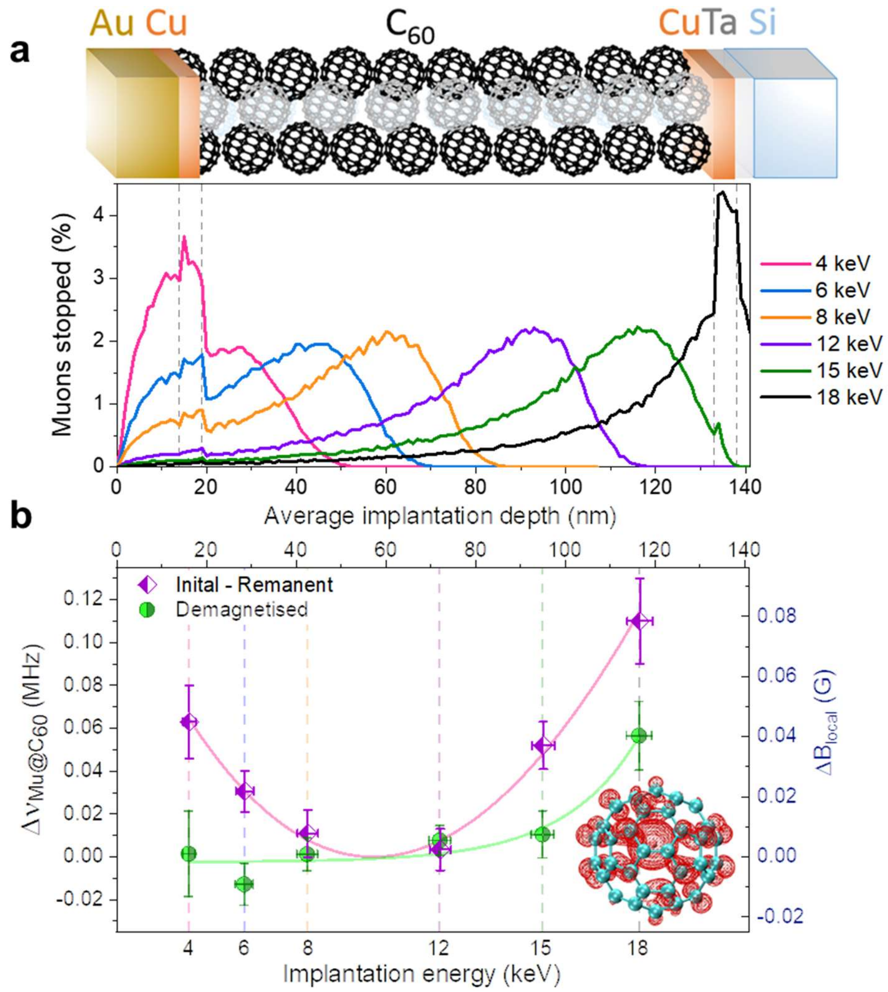

FIG. 4. *ZF-LE-μSR measurements of the Mu@*C_{60} *frequency,* υ_{Mu}*, and depth profile in a thin film heterostructure. (a) The simulated implantation profile for a structure of [Si(Sub)/Ta(3)/Cu(5)/*C_{60}*(114)/ Cu(5)/Au(14)], where the thicknesses in brackets are in nm. At the 4 and 18 keV implantation energies, a considerable percentage (57% and 34% respectively) of muons stop in the metal layers. As the measurement was performed in ZF, these are not expected to contribute to the oscillating signal. (b) The obtained depth dependence of the relative change in the* $ENDO_f$ *oscillation frequency,* $\Delta\upsilon_{Mu}$*, for the initial state measurement and following a degauss –lines are a guide for the eye. The corresponding change in the local field,* ΔB_{Local}*, calculated from the measured calibration curve in the crystalline* C_{60} *sample is also shown. Inset shows the highly anisotropic spin density (red:* $10^{-6}\ \mu_B\ \AA^{-3}$*) for the endohedral muonium polaron state with an additional electron* $ENDO_f$*(-) calculated using screened-hybrid DFT (HSE06, see SI).*

To examine the origin of the frequency shifts at the metallo-molecular interfaces, we compare the as-grown state with the signal after the sample is degaussed in a damped alternating field starting at 300 G. Following this degauss procedure, the depth profile of the muonium frequency dramatically changes. As shown in Fig. 4(b), υ_{Mu} now remains almost constant throughout the molecular layer. The increased υ_{Mu} frequency at both metal interfaces before degauss is therefore a consequence of Zeeman splitting of the muonium hyperfine levels due to small stray fields, of the order of 20-80 mG, originating at the Cu/C_{60} interface. After degauss, the remaining 9±3% frequency shift at the depth closest to the bottom Cu/C_{60} interface can be attributed to metal-to-molecule electron transfer at the interface and the presence of negatively charged $ENDO_f$(-). This state has a more anisotropic spin-density, leading to higher oscillation frequency (Inset in Fig. 4b and Sup. Mat. Fig. S11). The fact that there is no change in υ_{Mu} at the top Cu/C_{60} interface after degauss suggests a lower coupling and damage of the molecular layer with the metal layer sputtered on top as compared to the bottom interface, where the molecules were evaporated on the metal.

VI. CONCLUSION

We have presented LE-μSR data that characterises the dynamics of the endohedral floating muonium polaronic state in C_{60} layers. The hyperfine frequencies of this state map the emergent magnetism formed at a Cu/C_{60} interface via the Zeeman splitting of the muonium hyperfine coupling. DFT calculations were used to model the charge, spin density and dynamics of this muonium state, confirming it as the only system being detectable for temperatures > 260 K as observed in the experiments. The polaron state causes a small anisotropy in the hyperfine coupling of the endohedral muonium, which allows us to observe a zero-field precession of a few hundred kHz. This precession is very sensitive to any deviation from zero-field and therefore is highly sensitive to weak stray magnetic fields of weak or dilute magnetic moments. For a non-polaronic, isotropic muonium state, to measure a precession we need to apply a magnetic field. X-ray-based synchrotron techniques have been used to observe magnetic moments in Cu as small as 10^{-5} μ_B, which is roughly equivalent to local fields of 0.1 G.[5,6] The $ENDO_f$ polaronic state can detect local magnetic fields of ~0.01 Gauss and the charge transfer at a metallo-molecular interface (Fig. 4b). Where X-ray techniques are element sensitive, the muonium polaron offers the possibility to map the depth profile of the magnetisation and the distribution of free charge in e.g. magnetic multilayers, hybrid batteries or photovoltaic devices. C_{60} or other compounds forming muon polaron states such as crystalline semiconductors or oxides[37] are part of, or can be added, to the device structure.[7,8] For example, fullerene layers can be evaporated *in-situ* on top of candidates to 2-dimensional magnetism or ferroelectric materials to study weak surface effects such as magnetic monopoles.[14]

[1] C. Barraud, P. Seneor, R. Mattana, S. Fusil, K. Bouzehouane, C. Deranlot, P. Graziosi, L. Hueso, I. Bergenti, V. Dediu, F. Petroff, and A. Fert, Unravelling the role of the interface for spin injection into organic semiconductors, Nature Physics **6**, 615 (2010).

[2] M. Cinchetti, V. A. Dediu, and L. E. Hueso, Activating the molecular spinterface, Nat. Mater. **16**, 507 (2017).

[3] F. Al Ma'Mari, T. Moorsom, G. Teobaldi, W. Deacon, T. Prokscha, H. Luetkens, S. Lee, G. E. Sterbinsky, D. A. Arena, D. A. MacLaren, M. Flokstra, M. Ali, M. C. Wheeler, G. Burnell, B. J. Hickey, and O. Cespedes, Beating the Stoner criterion using molecular interfaces, Nature **524**, 69 (2015).

[4] F. Al Ma'Mari, M. Rogers, S. Alghamdi, T. Moorsom, S. Lee, T. Prokscha, H. Luetkens, M. Valvidares, G. Teobaldi, M. Flokstra, R. Stewart, P. Gargiani, M. Ali, G. Burnell, B. J. Hickey, and O. Cespedes, Emergent magnetism at transition-metal-nanocarbon interfaces, Proc. Natl. Acad. Sci. U.S.A. **114**, 5583 (2017).

[5] J. Li, L. R. Shelford, P. Shafer, A. Tan, J. X. Deng, P. S. Keatley, C. Hwang, E. Arenholz, G. van der Laan, R. J. Hicken, and Z. Q. Qiu, Direct Detection of Pure ac Spin Current by X-Ray Pump-Probe Measurements, Phys. Rev. Lett. **117**, 076602 (2016).

[6] R. Kukreja, S. Bonetti, Z. Chen, D. Backes, Y. Acremann, J. A. Katine, A. D. Kent, H. A. Durr, H. Ohldag, and J. Stohr, X-ray Detection of Transient Magnetic Moments Induced by a Spin Current in Cu, Phys. Rev. Lett. **115**, 096601 (2015).

[7] Y. H. Xiao, Y. Wang, S. H. Bo, J. C. Kim, L. J. Miara, and G. Ceder, Understanding interface stability in solid-state batteries, Nature Reviews Materials **5**, 105 (2020).

[8] T. Gatti, E. Menna, M. Meneghetti, M. Maggini, A. Petrozza, and F. Lamberti, The Renaissance of fullerenes with perovskite solar cells, Nano Energy **41**, 84 (2017).

[9] U. Binninger, C. Bernhard, A. Hofer, C. Niedermayer, E. Recknagel, J. Erxmeyer, and A. Weidinger, ROTATIONAL-DYNAMICS OF SOLID C-70 INVESTIGATED BY THE MUON-SPIN-ROTATION TECHNIQUE, Phys. Rev. B **51**, 14867 (1995).

[10] K. Prassides, T. J. S. Dennis, C. Christides, E. Roduner, H. W. Kroto, R. Taylor, and D. R. M. Walton, MU-AT-THE-COST-OF-C70 - MONITORING THE DYNAMICS OF FULLERENES FROM INSIDE THE CAGE, J. Phys. Chem. **96**, 10600 (1992).

[11] R. F. Kiefl, T. L. Duty, J. W. Schneider, A. Macfarlane, K. Chow, J. W. Elzey, P. Mendels, G. D. Morris, J. H. Brewer, E. J. Ansaldo, C. Niedermayer, D. R. Noakes, C. E. Stronach, B. Hitti, and J. E. Fischer, EVIDENCE FOR ENDOHEDRAL MUONIUM IN KXC60 AND CONSEQUENCES FOR ELECTRONIC-STRUCTURE, Phys. Rev. Lett. **69**, 2005 (1992).

[12] A. Lappas, K. Prassides, K. Vavekis, D. Arcon, R. Blinc, P. Cevc, A. Amato, R. Feyerherm, F. N. Gygax, and A. Schenck, SPONTANEOUS MAGNETIC-ORDERING IN THE FULLERENE CHARGE-TRANSFER SALT (TDAE)C-60, Science **267**, 1799 (1995).

[13] A. J. Drew, J. Hoppler, L. Schulz, F. L. Pratt, P. Desai, P. Shakya, T. Kreouzis, W. P. Gillin, A. Suter, N. A. Morley, V. K. Malik, A. Dubroka, K. W. Kim, H. Bouyanfif, F. Bourqui, C. Bernhard, R. Scheuermann, G. J. Nieuwenhuys, T. Prokscha, and E. Morenzoni, Direct measurement of the electronic spin diffusion length in a fully functional organic spin valve by low-energy muon spin rotation, Nat. Mater. **8**, 109 (2009).

[14] Q. N. Meier, M. Fechner, T. Nozaki, M. Sahashi, Z. Salman, T. Prokscha, A. Suter, P. Schoenherr, M. Lilienblum, P. Borisov, I. E. Dzyaloshinskii, M. Fiebig, H. Luetkens, and N. A. Spaldin, Search for the Magnetic Monopole at a Magnetoelectric Surface, Phys. Rev. X **9**, 011011 (2019).

[15] A. Di Bernardo, Z. Salman, X. L. Wang, M. Amado, M. Egilmez, M. G. Flokstra, A. Suter, S. L. Lee, J. H. Zhao, T. Prokscha, E. Morenzoni, M. G. Blamire, J. Linder, and J. W. A. Robinson, Intrinsic Paramagnetic Meissner Effect Due to s-Wave Odd-Frequency Superconductivity, Phys. Rev. X **5**, 041021 (2015).

[16] M. G. Flokstra, R. Stewart, N. Satchell, G. Burnell, H. Luetkens, T. Prokscha, A. Suter, E. Morenzoni, S. Langridge, and S. L. Lee, Observation of Anomalous Meissner Screening in Cu/Nb and Cu/Nb/Co Thin Films, Phys. Rev. Lett. **120**, 247001 (2018).

[17] See Supplemental Material at [URL will be inserted by publisher] for for further details on sample structure, low energy muon spin spectroscopy measurements, simulation of spectral intensities and DFT methods, which

includes Refs. [38-40, 42-75].
[18] W. I. F. David, R. M. Ibberson, T. J. S. Dennis, J. P. Hare, and K. Prassides, STRUCTURAL PHASE-TRANSITIONS IN THE FULLERENE C-60, Europhysics Letters **18**, 219 (1992).
[19] P. A. Heiney, J. E. Fischer, A. R. McGhie, W. J. Romanow, A. M. Denenstein, J. P. McCauley, A. B. Smith, and D. E. Cox, ORIENTATIONAL ORDERING TRANSITION IN SOLID C60, Phys. Rev. Lett. **66**, 2911 (1991).
[20] M. S. Dresselhaus, G. Dresselhaus, and P. C. Eklund, Science of Fullerenes and Carbon Nanotubes, Academic Press, 1682 (1996).
[21] T. L. Duty, J. H. Brewer, K. Chow, R. F. Kiefl, A. W. Macfarlane, G. D. Morris, J. W. Schneider, B. Hitti, R. Lichti, L. Brard, J. E. Fischer, A. B. Smith, and R. M. Strongin, ZERO-FIELD MU-SR IN CRYSTALLINE C-60, Hyperfine Interact. **86**, 789 (1994).
[22] R. F. Kiefl, J. W. Schneider, A. Macfarlane, K. Chow, T. L. Duty, T. L. Estle, B. Hitti, R. L. Lichti, E. J. Ansaldo, C. Schwab, P. W. Percival, G. Wei, S. Wlodek, K. Kojima, W. J. Romanow, J. P. McCauley, N. Coustel, J. E. Fischer, and A. B. Smith, MOLECULAR-DYNAMICS OF THE MUONIUM-C60 RADICAL IN SOLID C-60, Phys. Rev. Lett. **68**, 2708 (1992).
[23] E. J. Ansaldo, C. Niedermayer, and C. E. Stronach, MUONIUM IN FULLERITE, Nature **353**, 121 (1991).
[24] S. Gonda, M. Kawasaki, T. Arakane, and H. Koinuma, in *Novel Forms of Carbon Ii*, edited by C. L. Renschler *et al.*1994), pp. 325.
[25] Z. Salman, T. Prokscha, A. Amato, E. Morenzoni, R. Scheuermann, K. Sedlak, and A. Suter, Direct Spectroscopic Observation of a Shallow Hydrogenlike Donor State in Insulating SrTiO3, Phys. Rev. Lett. **113**, 156801 (2014).
[26] E. Abou-Hamad, Y. Kim, T. Wagberg, D. Boesch, S. Aloni, A. Zettl, A. Rubio, D. E. Luzzi, and C. Goze-Bac, Molecular Dynamics and Phase Transition in One-Dimensional Crystal of C-60 Encapsulated Inside Single Wall Carbon Nanotubes, Acs Nano **3**, 3878 (2009).
[27] I. McKenzie and S. P. Cottrell, Microscopic muon dynamics in the polymer electrolyte poly(ethylene oxide), Phys. Rev. E **96**, 012502 (2017).
[28] P. Jain, A. Levchenko, P. Yu, and S. Sen, Molecular dynamics in supercooled glycerol: Results from C-13 NMR spectroscopy, J. Chem. Phys. **130**, 194506 (2009).
[29] S. Adhikari, M. Selmke, and F. Cichos, Temperature dependent single molecule rotational dynamics in PMA, Phys. Chem. Chem. Phys. **13**, 1849 (2011).
[30] B. D. Patterson, MUONIUM STATES IN SEMICONDUCTORS, Rev. Mod. Phys. **60**, 69 (1988).
[31] J. A. Larsson, S. D. Elliott, J. C. Greer, J. Repp, G. Meyer, and R. Allenspach, Orientation of individual C-60 molecules adsorbed on Cu(111): Low-temperature scanning tunneling microscopy and density functional calculations, Phys. Rev. B **77**, 115434 (2008).
[32] W. W. Pai, H. T. Jeng, C. M. Cheng, C. H. Lin, X. D. Xiao, A. D. Zhao, X. Q. Zhang, G. Xu, X. Q. Shi, M. A. Van Hove, C. S. Hsue, and K. D. Tsuei, Optimal Electron Doping of a C-60 Monolayer on Cu(111) via Interface Reconstruction, Phys. Rev. Lett. **104**, 036103 (2010).
[33] G. Xu, X. Q. Shi, R. Q. Zhang, W. W. Pai, H. T. Jeng, and M. A. Van Hove, Detailed low-energy electron diffraction analysis of the (4 x 4) surface structure of C-60 on Cu(111): Seven-atom-vacancy reconstruction, Phys. Rev. B **86**, 075419 (2012).
[34] L. Martin-Olivera, D. G. Shchukin, and G. Teobaldi, Role of Metal Lattice Expansion and Molecular pi-Conjugation for the Magnetic Hardening at Cu-Organics Interfaces, J. Phys. Chem. C **121**, 23777 (2017).
[35] C. C. Chancey and M. C. M. O'Brien, The Jahn-Teller Effect in C60 and Other Icosahedral Complexes, Princeton University Press, 97 (1997).
[36] C. Niedermayer, Fullerenes with mu SR, Hyperfine Interact. **97-8**, 287 (1996).
[37] M. H. Dehn, J. K. Shenton, S. Holenstein, Q. N. Meier, D. J. Arseneau, D. L. Cortie, B. Hitti, A. C. Y. Fang, W. A. MacFarlane, R. M. L. McFadden, G. D. Morris, Z. Salman, H. Luetkens, N. A. Spaldin, M. Fechner, and R. F. Kiefl, Observation of a Charge-Neutral Muon-Polaron Complex in Antiferromagnetic Cr2O3, Phys. Rev. X **10**, 011036 (2020).
[38] T. Prokscha, E. Morenzoni, C. David, A. Hofer, H. Gluckler, and L. Scandella, Moderator gratings for the generation of epithermal positive muons, Appl. Surf. Sci. **172**, 235 (2001).
[39] T. Prokscha, E. Morenzoni, K. Deiters, F. Foroughi, D. George, R. Kobler, A. Suter, and V. Vrankovic, The new mu E4 beam at PSI: A hybrid-type large acceptance channel for the generation of a high intensity surface-muon beam, Nuclear Instruments & Methods in Physics Research Section a-Accelerators Spectrometers Detectors and Associated Equipment **595**, 317 (2008).

[40] E. Morenzoni, H. Glucker, T. Prokscha, R. Khasanov, H. Luetkens, M. Birke, E. M. Forgan, C. Niedermayer, and M. Pleines, Implantation studies of keV positive muons in thin metallic layers, Nucl. Instrum. Meth. B **192**, 254, Pii s0168-583x(01001166-1 (2002).
[41] R. M. Macrae, K. Prassides, I. M. Thomas, E. Roduner, C. Niedermayer, U. Binninger, C. Bernhard, A. Hofer, and I. D. Reid, REORIENTATIONAL DYNAMICS OF SOLID C-70 PROBED BY POSITIVE MUONS, J. Phys. Chem. **98**, 12133 (1994).
[42] T. Moorsom, M. Rogers, I. Scivetti, S. Bandaru, G. Teobaldi, M. Valvidares, M. Flokstra, S. Lee, R. Stewart, T. Prokscha, P. Gargiani, N. Alosaimi, G. Stefanou, M. Ali, F. Al Ma'Mari, G. Burnell, B. J. Hickey, and O. Cespedes, Reversible spin storage in metal oxide-fullerene heterojunctions, Science Advances **6**, eaax1085 (2020).
[43] J. S. Lord, Computer simulation of muon spin evolution, Physica B-Condensed Matter **374**, 472 (2006).
[44] S. K. Zaremba, Good lattice points, discrepancy, and numerical integration, Ann. Mat. Pura Appl. **4**, 293 (1966).
[45] H. Conroy, MOLECULAR SCHRODINGER EQUATION .8. A NEW METHOD FOR EVALUATION OF MULTIDIMENSIONAL INTEGRALS, J. Chem. Phys. **47**, 5307 (1967).
[46] V. B. Cheng, H. H. Suzukawa, and M. Wolfsberg, INVESTIGATIONS OF A NONRANDOM NUMERICAL-METHOD FOR MULTIDIMENSIONAL INTEGRATION, J. Chem. Phys. **59**, 3992 (1973).
[47] G. Kresse and J. Furthmuller, Efficient iterative schemes for ab initio total-energy calculations using a plane-wave basis set, Phys. Rev. B **54**, 11169 (1996).
[48] J. P. Perdew, K. Burke, and Y. Wang, Generalized gradient approximation for the exchange-correlation hole of a many-electron system, Phys. Rev. B **54**, 16533 (1996).
[49] S. Grimme, Semiempirical GGA-type density functional constructed with a long-range dispersion correction, Journal of Computational Chemistry **27**, 1787 (2006).
[50] G. Henkelman, B. P. Uberuaga, and H. Jonsson, A climbing image nudged elastic band method for finding saddle points and minimum energy paths, J. Chem. Phys. **113**, 9901, Pii [s0021-9606(00)71246-3] (2000).
[51] G. Henkelman and H. Jonsson, Improved tangent estimate in the nudged elastic band method for finding minimum energy paths and saddle points, J. Chem. Phys. **113**, 9978, Pii [s0021-9606(00)70546-0] (2000).
[52] A. V. Krukau, O. A. Vydrov, A. F. Izmaylov, and G. E. Scuseria, Influence of the exchange screening parameter on the performance of screened hybrid functionals, J. Chem. Phys. **125**, 224106 (2006).
[53] C. G. Van de Walle and J. Neugebauer, First-principles calculations for defects and impurities: Applications to III-nitrides, J. Appl. Phys. **95**, 3851 (2004).
[54] C. Freysoldt, B. Grabowski, T. Hickel, J. Neugebauer, G. Kresse, A. Janotti, and C. G. Van de Walle, First-principles calculations for point defects in solids, Rev. Mod. Phys. **86** (2014).
[55] E. Y. Kolyadina, L. A. Matveeva, P. L. Neluba, and E. F. Venger, Analysis of the fundamental absorption edge of the films obtained from the C-60 fullerene molecular beam in vacuum and effect of internal mechanical stresses on it, Semiconductor Physics Quantum Electronics & Optoelectronics **18**, 349 (2015).
[56] T. U. Ito, W. Higemoto, A. Koda, and K. Shimomura, Polaronic nature of a muonium-related paramagnetic center in SrTiO3, Appl. Phys. Lett. **115**, 192103 (2019).
[57] M. Reticcioli, M. Setvin, X. F. Hao, P. Flauger, G. Kresse, M. Schmid, U. Diebold, and C. Franchini, Polaron-Driven Surface Reconstructions, Phys. Rev. X **7**, 031053 (2017).
[58] T. D. Kuhne, M. Iannuzzi, M. Del Ben, V. V. Rybkin, P. Seewald, F. Stein, T. Laino, R. Z. Khaliullin, O. Schutt, F. Schiffmann, D. Golze, J. Wilhelm, S. Chulkov, M. H. Bani-Hashemian, V. Weber, U. Borstnik, M. Taillefumier, A. S. Jakobovits, A. Lazzaro, H. Pabst, T. Muller, R. Schade, M. Guidon, S. Andermatt, N. Holmberg, G. K. Schenter, A. Hehn, A. Bussy, F. Belleflamme, G. Tabacchi, A. Gloss, M. Lass, I. Bethune, C. J. Mundy, C. Plessl, M. Watkins, J. VandeVondele, M. Krack, and J. Hutter, CP2K: An electronic structure and molecular dynamics software package - Quickstep: Efficient and accurate electronic structure calculations, J. Chem. Phys. **152**, 194103 (2020).
[59] S. Goedecker, M. Teter, and J. Hutter, Separable dual-space Gaussian pseudopotentials, Phys. Rev. B **54**, 1703 (1996).
[60] J. VandeVondele and J. Hutter, Gaussian basis sets for accurate calculations on molecular systems in gas and condensed phases, J. Chem. Phys. **127**, 114105 (2007).
[61] S. Grimme, J. Antony, S. Ehrlich, and H. Krieg, A consistent and accurate ab initio parametrization of density functional dispersion correction (DFT-D) for the 94 elements H-Pu, J. Chem. Phys. **132**, 154104 (2010).
[62] D. Marx and M. Parrinello, Ab initio path integral molecular dynamics: Basic ideas, J. Chem. Phys. **104**, 4077 (1996).

[63] M. Ceriotti and D. E. Manolopoulos, Efficient First-Principles Calculation of the Quantum Kinetic Energy and Momentum Distribution of Nuclei, Phys. Rev. Lett. **109**, 100604 (2012).
[64] F. Uhl, D. Marx, and M. Ceriotti, Accelerated path integral methods for atomistic simulations at ultra-low temperatures, J. Chem. Phys. **145**, 054101 (2016).
[65] Y. Nagata, R. E. Pool, E. H. G. Backus, and M. Bonn, Nuclear Quantum Effects Affect Bond Orientation of Water at the Water-Vapor Interface, Phys. Rev. Lett. **109**, 226101 (2012).
[66] O. Marsalek and T. E. Markland, Ab initio molecular dynamics with nuclear quantum effects at classical cost: Ring polymer contraction for density functional theory, J. Chem. Phys. **144**, 054112 (2016).
[67] C. Schran, F. Brieuc, and D. Marx, Converged Colored Noise Path Integral Molecular Dynamics Study of the Zundel Cation Down to Ultralow Temperatures at Coupled Cluster Accuracy, Journal of Chemical Theory and Computation **14**, 5068 (2018).
[68] S. J. Clark, M. D. Segall, C. J. Pickard, P. J. Hasnip, M. J. Probert, K. Refson, and M. C. Payne, First principles methods using CASTEP, Zeitschrift Fur Kristallographie **220**, 567 (2005).
[69] J. P. Perdew, K. Burke, and M. Ernzerhof, Generalized gradient approximation made simple (vol 77, pg 3865, 1996), Phys. Rev. Lett. **78**, 1396 (1997).
[70] J. S. Lin, A. Qteish, M. C. Payne, and V. Heine, OPTIMIZED AND TRANSFERABLE NONLOCAL SEPARABLE ABINITIO PSEUDOPOTENTIALS, Phys. Rev. B **47**, 4174 (1993).
[71] H. J. Monkhorst and J. D. Pack, SPECIAL POINTS FOR BRILLOUIN-ZONE INTEGRATIONS, Phys. Rev. B **13**, 5188 (1976).
[72] B. S. Hudson and S. K. Chafetz, Zero-Point Corrections for Isotropic Coupling Constants for Cyclohexadienyl Radical, C6H7 and C(6)H(6)Mu: Beyond the Bond Length Change Approximation, Molecules **18**, 4906 (2013).
[73] I. McKenzie, J. C. Brodovitch, P. W. Percival, T. Ramnial, and J. A. C. Clyburne, The reactions of imidazol-2-ylidenes with the hydrogen atom: A theoretical study and experimental confirmation with muonium, J. Am. Chem. Soc. **125**, 11565 (2003).
[74] C. H. Yue, L. Liborio, T. Bian, S. Sturniolo, J. Wright, S. P. Cottrell, R. Khasanov, G. Simutis, U. A. Jayasooriya, and Y. Chao, A Muon Spectroscopic and Computational Study of the Microscopic Electronic Structure in Thermoelectric Hybrid Silicon Nanostructures, J. Phys. Chem. C **124**, 9656 (2020).
[75] J. S. Moller, D. Ceresoli, T. Lancaster, N. Marzari, and S. J. Blundell, Quantum states of muons in fluorides, Phys. Rev. B **87**, 121108 (2013).

Methods

For all measured samples, metal films were deposited by DC magnetron sputtering and C_{60} films were sublimated in a high vacuum system with a 10^{-8} mbar base pressure. Sputtering was undertaken in a 3.3×10^{-3} mbar Ar atmosphere at ambient temperature unless otherwise specified. The growth rate of each material was calibrated against samples grown in the same vacuum cycle whose thickness was determined via the fitting of Kiessig fringes produced by X-ray reflectivity measurements.

LE-μSR measurements were performed on the μE4 beamline at the Paul Scherrer Institute, where a moderator technique allows for the implantation energy of nearly 100% spin polarised epithermal muons to be tuned via an acceleration electric field.[38,39] Thus, low-energy muons allow for the depth profile of magnetic texture to be obtained. The energies required to probe the Cu/C_{60} were determined through the use of Monte Carlo simulations performed within TRIM.SP software.[40] The muon is an unstable spin ½ particle with charge +*e* and a lifetime of $\tau_\mu \sim 2.2$ μs. Following implantation, the muon will rapidly thermalise. In a system which lacks sufficient carrier concentration to screen the μ^+ charge, such as insulating and semiconducting systems, the muon is expected to generate a hydrogen-like bound state known as muonium (Mu=μ^+e^-). In a metallic system, one would observe the Larmour spin precession of the μ^+ particle about a local field B_{loc}. In a system where the muonium formation dominates the signal, we directly probe transitions between spin configurations of the μ^+ and e^- spin, governed by the Hamiltonian which describes the hyperfine interaction. This is given, in terms of angular frequency, as

$$\frac{H_{HF}}{\hbar} = -\gamma_\mu \boldsymbol{S}^\mu \cdot \boldsymbol{B} + \gamma_e \boldsymbol{S}^e \cdot \boldsymbol{B} + \boldsymbol{S}^\mu \cdot A \cdot \boldsymbol{S}^e \quad (4)$$

where $\mathbf{S}^\mu$ and $\mathbf{S}^e$ are the respective muon and electron spin operators, γ_μ and γ_e are the gyromagnetic ratios for the electron and muon, A is the hyperfine coupling tensor and **B** is the magnetic field.[30,41] For an isotropic hyperfine tensor ($A_{xx} = A_{yy} = A_{zz}$), two states exist in zero-field: a singlet and a degenerate triplet state. The application of a magnetic field lifts the degeneracy of the triplet state and then transitions between energy levels can be observed as an oscillation frequency v_{ij} which is equal to the splitting between energy levels $(E_i - E_j)/\hbar$. The splitting between the zero-field (ZF) states is equal to the hyperfine coupling constant $A_H = 2\pi \times 4463$ MHz. This frequency would be unobservable in a typical μSR experiment. Therefore, it is expected that no oscillation should be observed in the isotropic hyperfine case. If, however, some axial anisotropy is introduced into the hyperfine tensor, the degeneracy of the triplet state is lifted and a single frequency can now be expected in the absence of magnetic field. The μSR data were analysed using the program musrfit[36].

Acknowledgements

We thank the Engineering and Physical Sciences Research Council (EPSRC UK) for support via grants no. EP/M000923/1, EP/K036408/1, EP/I004483/1, EP/S031081/1, and EP/S030263/1. L.L., S.S., D.J. and G.T. acknowledge also support from STFC-ISIS Neutron and Muon Source and Ada Lovelace Centre at STFC-SCD. We acknowledge use of the ARCHER (via the UK Car–Parrinello Consortium, EP/P022618/1 and EP/P022189/2), UK Materials and Molecular Modelling Hub (EP/P020194/1), and STFC Scientific Computing Department's SCARF HCP facilities. The LE-μSR measurements were performed at the Swiss Muon Source SμS, Paul Scherrer Institute, Villigen, Switzerland.